# *Operando* Methods for the Mechanistic Elucidation of an Electrochemically Driven Structural Transformation

E. Martínez-Periñán[†], M. Revenga-Parra[†,‡,§], J. Pastore[‖], F. Pariente[†,‡], F. Zamora[ǂ,‡,§], O. Castillo[ǂ], E. Lorenzo[†,‡,§] and H. D. Abruña[‖ *]

[†]Departamento de Química Analítica, [ǂ]Departamento de Química Inorgánica and [‡]Institute for Advanced Research in Chemical Sciences (IAdChem), Universidad Autónoma de Madrid, 28049, Madrid, Spain

[§]Instituto Madrileño de Estudios Avanzados en Nanociencia (IMDEA Nanociencia), Cantoblanco, 28049 Madrid, Spain.

[‖]Department of Chemistry and Chemical Biology, Cornell University, Ithaca, New York 14853, USA.

[ǂ]Departamento de Química Inorgánica, Universidad del País Vasco. Apartado 644, e–48080 Bilbao, Spain.

*Corresponding author. Tel.: +1 (607) 255-4720; Fax: +1 (607) 255-9864

E-mail address: hda1@cornell.edu (H. D. Abruña)

Postal address: Department of Chemistry and Chemical Biology, Cornell University, Ithaca, New York 14853, USA.

**Abstract**

We present the use of operando methods for the mechanistic dilucidation of an electrochemically driven structural transformation of a Ni(II) thioacetate complex. Specifically, we employed operando Raman spectroscopy and electrochemistry, along with X-ray diffraction to characterize the electrochemically induced conversion of a paddle–wheel tetrakis-acetate dinickel (II) complex into the related di-nickel acetate. Successive Raman spectra were obtained from the surface of a gold electrode immersed in an electrochemical cell containing the dinuclear complex $[Ni_2(CH_3COS)_4 \cdot EtOH]$ under a constant applied potential, to oxidize the complex, and effects its conversion/transformation into the unprecedented $[Ni(CH_3COO)_2]_n$ electrodeposited onto the electrode surface as microstructures. The crystal structure of the new electrogenerated compound $[Ni(CH_3COO)_2]_n$ was also examined by synchrotron X-ray diffraction. The observation of a disulfide species, generated during the electrochemical process *via* Raman spectroscopy was consistent with and served to confirm the proposed mechanism. These approaches can be readily applied to numerous electrode potential induced transformations.

**Introduction.**

*Operando* techniques are growing in importance with the realization that *ex situ* methods only provide limited details of dynamics. In particular, *operando* methods in electrochemistry[1-6] are providing realistic details on a myriad of processes. The development of *operando* methods, which operate under potential control, can help identify reaction products and offer great insights on electrochemical processes. Among these, Raman spectroelectrochemistry has been widely used for the investigation of electrochemically generated intermediates and products. It can provide valuable mechanistic information about species electrogenerated in solution, or adsorbed[7] or electrodeposited[8] on the electrode surfaces[9]. In addition, Surface-enhanced Raman scattering (SERS) is a powerful analytical tool for sensitive and selective detection of molecules adsorbed on nanostructured metals[10], especially silver and gold. Thus, molecules present at the electrode surface at low coverage can be detected due to dramatic increase in signal[9].

We have recently reported on the generation of metal-organic microstructures, using electrochemistry as an alternative synthetic procedure, that precludes contamination[11]. Specifically, we studied a paddle-wheel dinickel tetrakis-thioacetate complex, $[Ni_2(CH_3COS)_4 \cdot EtOH]$ **1**, as precursor in an electrodeposition process yielding nickel based microstructures on different electrode surfaces[11] to finally form (by alkaline treatment) on-surface nickel hydroxide nanoparticles with a potent and persistent electrocatalytic activity towards the oxidation of different sugars and alcohols. The electrodeposited structures have been characterized by X-ray Photoelectron Spectroscopy (XPS) and mass spectrometry, which indicated the formation of a novel Ni(II) acetate complex, $[Ni(CH_3COO)_2]_n$ **2**. No methods for the chemical synthesis of this complex, in solution, have been reported so far. Based on these data, we proposed an electrochemical

mechanism in which a four-electron oxidation process results in the transformation/conversion of compound **1** into **2** (Scheme 1). Indeed, each sulfur atom in the starting material loses one electron, resulting in the formation of a polysulfide species. However, although electrochemical techniques can provide evidence about reaction mechanisms and potential reaction intermediates, a full description and analysis often requires the use of complementary techniques; especially spectroscopic and structural.

In the present work, we have carried out *operando* confocal Raman spectroscopy during the electrochemical reaction to elucidate the mechanism, by which the microstructures described above are electrogenerated at gold electrode surfaces. In addition, we have employed synchrotron X-ray diffraction (SXRD) methods to characterize structural aspects of this electrode potential induced transformation

The specific system under study can be considered as an example of the application of new materials as precursors for electrode modification at the sub-micron or nanoscale. Depending on the precursor used, the resulting electrodeposited material could be employed in different applications. A knowledge of mechanistic details would, in principle, enable control of the process and the resulting structures/materials.

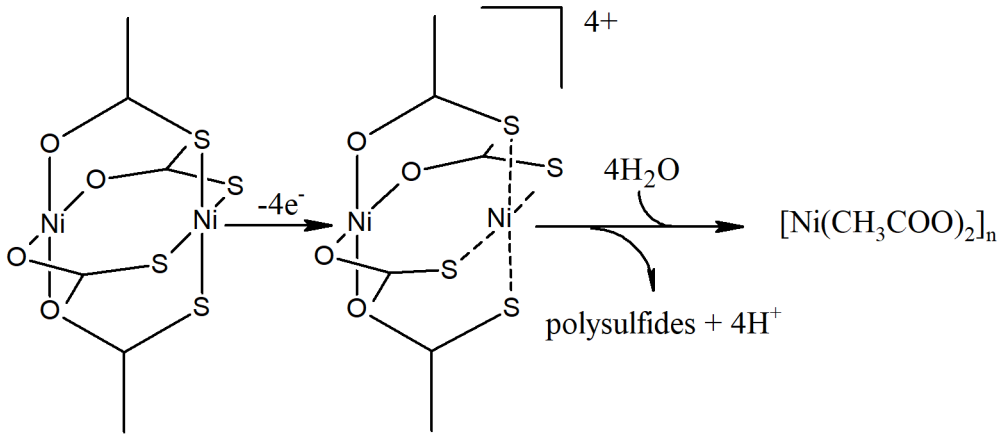


**Scheme 1**. Proposed electrochemical mechanism for the electrodeposition process of $[Ni(CH_3COO)_2]_n$ **2** using $[Ni_2(CH_3COS)_4 \cdot EtOH]$ **1** as precursor.

## Experimental Section

Anhydrous chloroform ($CHCl_3$) and tetrabutylammonium perchlorate (TBAP), for electrochemical analysis were purchased from Sigma-Aldrich and were used as received. $[Ni_2(CH_3COS)_4 \cdot EtOH]$ **1** was prepared as previously described [11]. For conventional electrochemical measurements and *operando* Raman spectroscopic and electrochemical measurements, $2.5 \times 10^{-4}$ M solutions of **1** in 0.1 M TBAP/$CHCl_3$ were employed.

The gold electrodes used for electrodepositing **2** from **1** electrooxidation were glass (1.1 cm × 1.1 cm) covered with evaporated gold layers (0.2-0.3 μm) deposited over a chromium adhesion layer (Gold arrandee™) suited for the flame annealing (2 min in a gas flame) procedure which is used to obtain Au (111) terraces. These gold electrodes were previously cleaned with "piranha" solution (3:1 concentrated $H_2SO_4$:30% $H_2O_2$) followed by exhaustive rinsing with ultrapure water. Caution: piranha solution reacts violently with most organic materials and may result in explosion or skin burns if not handled with extreme caution.

The electrosynthesis of **2** was carried out applying a constant potential of 1.20 V *vs.* SCE during 7200 s with the electrode immersed in a $2.5\times10^{-4}$ M solution of **1** in 0.1 M TBAP/ $CHCl_3$. Once the electrodeposition step is completed the gold surfaces were rinsed with clean chloroform in order to eliminate the exceed of compound **1**.

X-ray diffraction of electrodeposited **2** over gold electrodes (as it as been described above) was carried out on beamline A-3 at the Cornell High Energy Synchrotron Source using 19.KeV incident radiation.

All electrochemical measurements and the electrosynthesis of **2** were performed with an Autolab PGSTAT128N potentiostat (EcoChemie, NL) using the software package NOVA 1.5. For conventional three electrode experiments, a homemade single compartment electrochemical cell was employed. Gold disk electrodes, from CH Instruments, were used as working electrodes and a large area Pt wire served as counter electrode. An Ag wire was used as a quasi-reference electrode (QRE) for experiments in organic solvents. For gold electrode pretreatment, a saturated calomel reference electrode was employed.

*Ex situ* Raman experiments were carried out by confocal Raman spectroscopy of the modified gold electrode surfaces immersed in the appropriated solution before and after the electrochemical process (that is without potential control while Raman spectra were obtained). *Operando* Raman spectrophotometry during electrochemical measurements were carried out using a 3 electrode setup (Figure 1) previously described[8]. Polycrystalline gold electrodes used as working electrodes were polished with 600 mesh and subsequently with 1200 and 2000 mesh sandpaper and thoroughly rinsed with deionized water. An electrochemical cleaning procedure was carried out, consisting on the application of 30 cyclic voltammetric scans from -0.4 V to -2.0 V at 0.5 V $s^{-1}$ to the gold electrode immersed in 0.5 M KOH. The clean gold electrode was subsequently

activated in 0.5 M $H_2SO_4$ by applying cyclic voltammetric scans between -0.2 V to +1.5 V until the voltammetric profile of polycrystalline gold was obtained. Then, the gold disc electrodes were pretreated to generate gold nanoparticles in order to promote the SERS effect[12]. Pretreatment consisted on oxidation−reduction cycles in 0.1 M KCl in the potential range from −0.3 to +1.3 V *vs* saturated calomel electrode at a scan rate of 0.1 V $s^{-1}$ [13]. A coiled Pt wire and an Ag wire were employed as counter and a quasi-reference electrodes, respectively. Spectra were acquired simultaneously when the electrodeposition potential was applied. An inVia Renishaw confocal Raman spectrometer, using a 785 nm excitation wavelength laser at 0.1 % of the intensity, and with a 20× objective, in a Leica microscope, was employed.

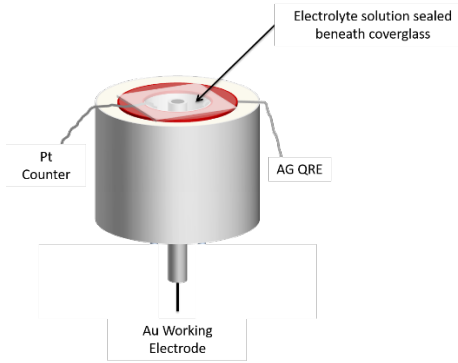


**Figure 1.** Schematic of the *in situ* Raman spectroelectrochemical cell used in the experiments.

**Results and discussion.**

*Crystal structure analysis of compound **2**.*

The crystal structure of **2** has not been previously described, and also the amounts obtained during the electrosynthesis process do not allow a conventional powder XRD analysis. Therefore, to elucidate the crystal structure of electrogenerated compound **2** and validate the proposed mechanism a more sensitive technique as SXRD analysis of the

final reaction product **2** were carried out (Figure 2). Sample was placed at grazing incidence and hit with photons at an energy of 19.78 keV. Figure 2 shows the diffractogram obtained for the analysis of a gold substrate in which it had been previously electrodeposited the compound **2**. The high intensity peak observed at 9º correspond to the reflected beam and the pair of peaks at approximately 15.5 and 17.5º are from the gold sputtered onto the silicon substrate. Therefore, there are only 8 suitable peaks which are usually considered an insufficient number of data to obtain reliable unit cell parameters. However, the analysis of the structural data for some other anhydrous metal acetates (Table 1) indicates that the unit cell-volume should be a multiple of 150-170 $Å^3$. Taking into account this structural information, it was possible to select a plausible unit cell from the huge amount of tentative unit cells coming from the indexing of the 8 diffraction peaks provided by the SXRD experiment (inset Figure 2).

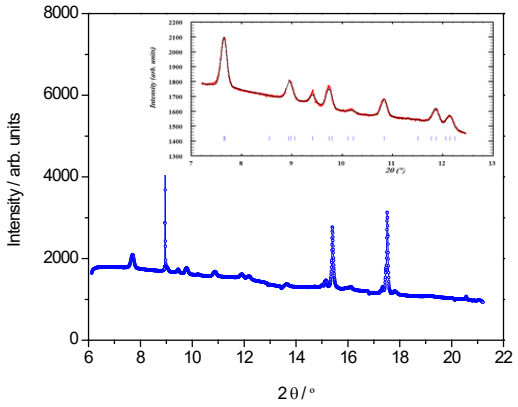


**Figure 2.** X-ray diffractogram of **2** crystals electrodeposited over gold electrodes. Inset: pattern-matching using the unit cell proposed in Table 1.

**Table 1.** Unit cell parameters of some anhydrous divalent transition metal acetates indicating the dimensionality of the coordination network.

| *Zinc(II) acetate* | a (Å) | b (Å) | c (Å) | α (º) | β (º) | γ (º) | V (Å$^3$) | Z | Ref. |
|---|---|---|---|---|---|---|---|---|---|
| F*dd2* (3D) | 15.712 | 15.558 | 10.901 | -- | -- | -- | 2664.7 | 16 | [14] |
| C*2/c* (2D) | 30.237 | 5.320 | 11.020 | -- | 100.00 | -- | 1325.3 | 8 | [15] |
| P$2_1$/*c* (2D) | 15.096 | 4.7967 | 9.2361 | -- | 98.10 | -- | 662.1 | 4 | [16] |
| *Iron(II) acetate* | | | | | | | | | |
| P*bcn* (2D) | 18.172 | 22.145 | 8.278 | -- | -- | -- | 3331.2 | 20 | [17] |
| *Cobalt(II) acetate* | | | | | | | | | |
| P*bcn* (2D) | 17.67 | 22.22 | 8.26 | -- | -- | -- | 3243.1 | 20 | [18] |
| *Chromium(II) acetate* | | | | | | | | | |
| $P\bar{1}$ (1D) | 7.583 | 8.688 | 5.178 | 111.16 | 95.77 | 98.16 | 310.6 | 2 | [19] |
| Plausible unit cell of compound **2**; *nickel(II) acetate* | | | | | | | | | |
| | 7.637 | 4.670 | 9.377 | | 90.88 | | 334.4 | 2 | This work |

Based on the reported crystal structures, there are two main architectures depending on the coordination mode of the acetate ligand. In the chromium anhydrous acetate, dinuclear units are clearly distinguishable in which the metal centers are bridged by four *syn-syn* coordinated acetate ligands[19]. These dimeric entities are further connected through semicoordination of an oxygen atom from an adjacent unit to the apical position of the metal center, leading to a 1D coordination polymer. The remaining examples comprising the iron(II), cobalt(II) and zinc(II) anhydrous acetates present more extended crystal structures in which the previously described dimeric subunits are not distinguishable. [14, 15, 17, 18]. The coordination geometry of the metal center differs from the tetrahedral environment found for the zinc polymorphs to the octahedral one observed for the cobalt and iron acetates. There is a close resemblance between the proposed unit cell compound

**2** with that of the zinc polymorph crystallizing in the P$2_1/c$ space group but with an *a* parameter half of the previous one and a more acute β angle. Therefore it seems quite plausible that the crystal structure of compound **2** is based also on a 2D extended coordination polymer (Figure 3) involving a *syn-anti* coordination mode for the acetate anion. It is worth to note that the diffraction pattern did not agree with the previously reported crystal structures of hydrated nickel acetates[20-22].

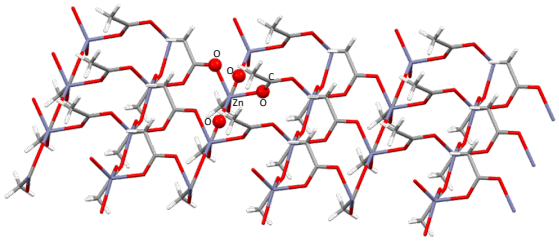


**Figure 3.** Representation of a polymeric layer of the closely related $[Zn(OOCCH_3)_2]_n$ monoclinic polymorph. The coordination environment around the metal center has been indicated for the sake of clarity.

*Operando Raman spectroscopy.*

The cyclic voltammetry of **1** in 0.1 M TBAP/$CHCl_3$ exhibits an irreversible oxidation process at about +0.85 V (Figure 4A). Cycling the potential from 0.0 to 1.5 V at 0.1 V $s^{-1}$ or holding the potential at 1.20 V results in a decrease in current, indicating that a non-conductive material is being electrodeposited on the electrode surface. The optical microscopy image of the resulting electrode surface shows that the material **2** is electrodeposited as needle-like crystals, randomly distributed on the gold surface (Figure 4B). By simply controlling the electrodeposition time, it is possible to change the size of the structures formed. The presence of trace water in the chloroform, used as solvent,

appears to increase surface coverage. This indicates that water plays an important role in the electrogeneration of these microstructures [11].

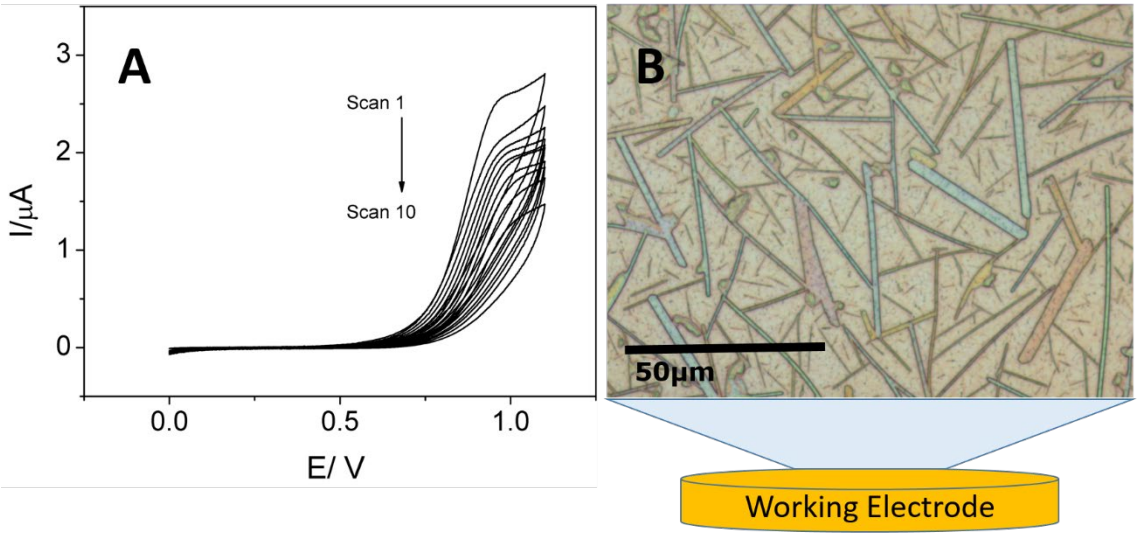


**Figure 4.** (A) Cyclic voltammetric scans of a $2.5\times10^{-4}$ M solution of **1** at an Au electrode in 0.1 M TBAP/ $CHCl_3$ at a scan rate of 0.1 V $s^{-1}$. (B) Optical microscopy image of electrodeposited **2** onto the gold electrode surface.

A wide scan overview XPS of the precursor on the surface (compound **1**) confirms its composition upon adsorption onto the gold surface. After **1** was electrochemically oxidized at +1.20 V for 300 s, and the electrodeposited microstructures of **2** are formed, the sulfur peak in the XPS spectra disappeared indicating the conversion from a monothiocarboxylate in the precursor into a carboxylate group in the product[11]. Furthermore, the binding energies of carbon and oxygen at 286.4 and 531.2 eV, respectively, confirm the presence of a carboxylate group. The Ni $2p^{1/2}$ peak appears at ca. 856.3 eV characteristic of a Ni(II) acetate complex [23].

Therefore, these results agree well with the absence of sulfur atoms in the microstructures and support that during the electrodeposition process, sulfur atoms are lost and the electrodeposited microstructures likely correspond to a Ni(II) acetate complex.

From coulometric measurements, the number of electrons involved in the overall process was determined to be 4. From the data obtained, it seems that the transformation of **1** to form **2** involves replacing all of the sulfur atoms by oxygen, and forming the corresponding polysulfide species, according to the process depicted in Scheme 1.

In order to obtain additional evidence of the proposed mechanism, we wanted to detect the electrode-surface-species formed under reaction conditions using both *ex situ* and *operando* Raman spectroscopic studies.

Raman spectra of a powdered sample of **1** deposited onto the Au surface and **2** initially electrodeposited onto an Au surface were obtained (Figure 5). Taking into account the molecular structure of the precursor **1** the peaks in Figure 5A could be assigned as follows: peaks at 177 $cm^{-1}$, 259 $cm^{-1}$ and 553 $cm^{-1}$ correspond to Ni-S bonds vibrations like $\nu^{B}$(Ni-S), $\nu^{A}$(Ni-S) and $\nu$(Ni-S), respectively. These are similar to Raman bands observed in nickel complexes coordinated by sulfur atoms in a planar disposition (194 $cm^{-1}$ $\nu^{B}$(Ni-S), 241 $cm^{-1}$ $\nu^{A}$(Ni-S) and 555 $cm^{-1}$ $\nu$(Ni-S))[24]. It is worth noting that these Raman shifts are very close to those of NiS, which appear at 174 $cm^{-1}$ and 246 $cm^{-1}$, respectively [25]. Moreover, the band at 222 $cm^{-1}$ present in NiS molecule [25], and which corresponds to a $\nu$(Ni-S) vibration is also detected in the Raman spectrum of **1** at 219 $cm^{-1}$. The less defined band, detected at 336 $cm^{-1}$, is close to the one detected at 328 $cm^{-1}$ by Siiman [24] for a nickel complex coordinated by sulfur atoms in a planar disposition, and is associated to the contribution of two torsional vibrations $\delta$(CCS)+ $\delta$(CCO)[24]. Ni-O vibrations, which Siiman detected at 398 $cm^{-1}$ [24], are observed here at 416 $cm^{-1}$ $\nu^{A}$(Ni-O). The band at 708 $cm^{-1}$ is assigned to $\nu$(C=S) and $\nu$(C-$CH_3$) vibrations. This is possible due

to the charge delocalization that involves the double bond (C=S) contribution of the resonant structure [24]. These Raman bands, assigned to a solid powder of **1** agree well with the molecular structure of the compound. The spectrum of the electrodeposited compound **2,** figure 5B, shows no bands involving sulfur atom bonds, which implies that there are no sulfur atoms in the electrodeposited material. The band at 460 $cm^{-1}$ is associated with a ν(Ni-O) vibration for a complex containing Ni-O bonds, in which only oxygen atoms coordinate the nickel center[26]. Raman peaks at 624 $cm^{-1}$ typically appear in acetate groups as a consequence of the torsional vibration δ(COO), as can be seen in the case of mononuclear nickel acetate [27]. Finally the band at 933 $cm^{-1}$ corresponds to the C-C bond of the acetate groups [27]. All Raman peaks are in good agreement with the proposed structure of **2**.

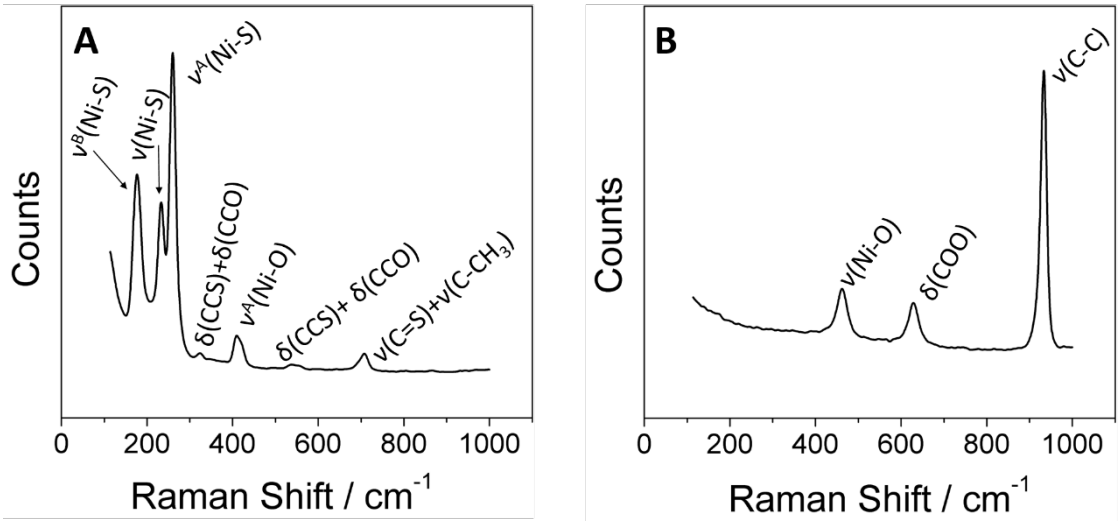


**Figure 5.** Raman spectra of a powdered sample of **1** (A) and **2** electrodeposited onto a gold electrode surface (B).

Figure 6 presents Raman spectra of a gold disc electrode immersed in different solutions in addition to the Raman spectra of a powdered sample **1** and **2** electrodeposited onto an Au electrode as described above. The spectrum obtained for the gold electrode immersed in 0.1 M TBAP/$CHCl_3$ (pink line) exhibits three intense bands associated with the solvent

(chloroform). When the electrode is immersed in a solution of 0.1 M TBAP/$CHCl_3$ containing $2.5 \cdot 10^{-4}$ M **1** (blue line), the same conditions as those used in the electrodeposition process, it can be seen that many of the Raman bands observed for **1** in powder form (red) appear, in addition to the solvent bands described above. In particular, bands at 222 $cm^{-1}$, 259 $cm^{-1}$ and 416 $cm^{-1}$ are likely observed. These bands are less intense than those ascribed to the solvent, due to the low concentration of the complex **1** in solution. The spectrum obtained after the electrodeposition process, by applying a potential of 1.20 V for 300 s, is presented in green. New bands with the same Raman shifts observed for the spectra of the electrodeposited material **2** (black) are evident. In particular, bands at 460 $cm^{-1}$ and 933$cm^{-1}$ appear in the spectrum of the modified electrode surface after electrodeposition, which are very similar to those observed in the Raman spectrum of the electrodeposited solid **2**. These results confirm that the electrodeposited material corresponds to the nickel acetate complex.

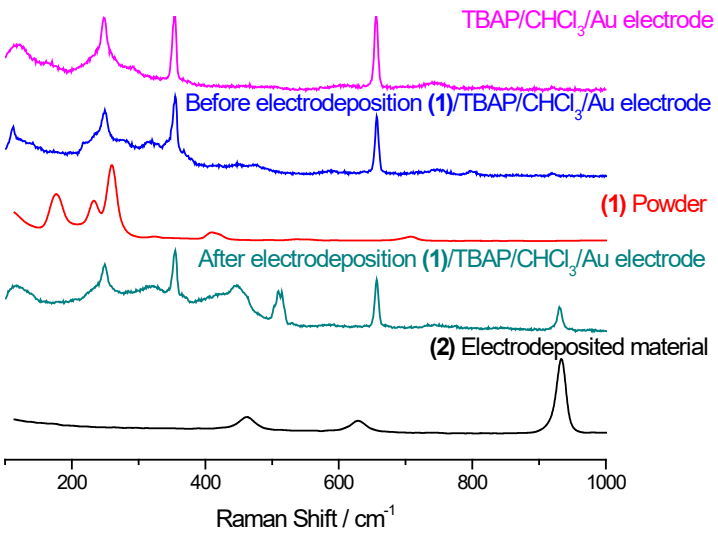


**Figure 6.** *Ex situ* Raman spectra of gold electrode immersed in: 0.1 M TBAP/$CHCl_3$ (pink), $2.5 \cdot 10^{-4}$ M **1**/0.1 M TBAP/$CHCl_3$ before electrodeposition (blue) and after

electrodeposition (green). Raman spectra of complex **1** powder (red) and electrodeposited complex **2** (black).

The proposed electrochemical mechanism for the electrogeneration of compound **2** from **1** (Scheme 1) was further confirmed by *operando* measurements in which the successive Raman spectra of the gold electrode surface immersed in the work solution ($2.5 \cdot 10^{-4}$ M **1**/0.1M TBAP/$CHCl_3$) under a constant applied potential of +1.20 V were obtained. Successive spectra were recorded every 25 seconds for 225 seconds, during which the electrodeposition process was carried out. *Operando* Raman spectra are presented in Figure 7. As the electrodeposition process went on, two Raman bands at 460 $cm^{-1}$ and 933 $cm^{-1}$ associated with complex **2** appeared, with their intensities increasing with increasing electrodeposition time. Moreover, an additional Raman band at 510 $cm^{-1}$ appeared. This band is not associated with either of the complexes **1** nor **2** nor with the medium (TBAP/ $CHCl_3$). Rather it appears at a frequency characteristic of the vibration of S-S bonds (ν(S-S) 510 $cm^{-1}$) which in the present context is ascribed to polysulfide species, which is a secondary reaction product in the proposed mechanism (Scheme 1). This result allows us to identify the nature of the main reaction intermediate, and confirm the electrochemical mechanism proposed for the generation of $[Ni(CH_3COO)_2]_n$ microstructures.

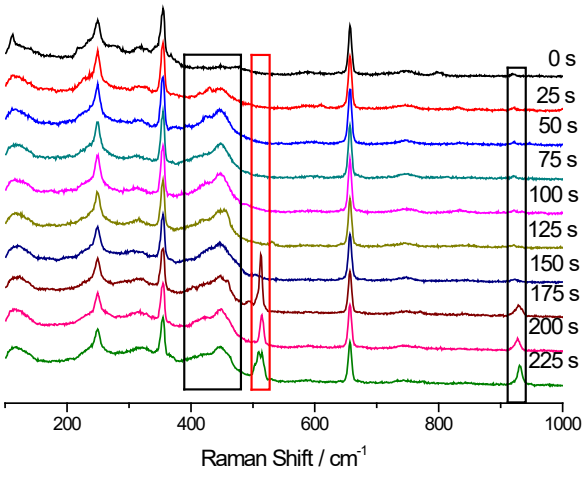

**Figure 6.** *Operando* Raman spectra of a gold electrode immersed in $2.5 \cdot 10^{-4}$ M **1**/0.1 M TBAP/$CHCl_3$ under 1.20 V.

## 4. Conclusions.

We have directly observed polysulfides formation in real time during the electrogeneration of a Ni based microstructures from electrooxidation of a dinickel tetrakis-thioacetate complex, $[Ni_2(CH_3COS)_4 \cdot EtOH]$ **1**, with *operando* Raman in order to elucidate the reaction mechanism. The above presented results illustrate that more authentic information and new insight into an electrochemical process such as the electrogeneration of a new compound as microstructures on electrode surfaces can be obtained when simultaneous *operando* Raman spectroscopy and electrochemistry is used instead of the respective separate *operando* techniques. Moreover, the SXRD results provide clear evidence that electrogenerated compound **2** is an 2D extended coordination polymer $[Ni(CH_3COO)_2]_n$. These microstructures are the starting material in a way to finally obtain highly dense surface coverages of NiO nanoparticles, which act as potent electrocatalyst towards sugars and alcohols oxidation.

**Acknowledgements.** Funding from the Spanish MICINN (projects. CTQ2014-53334-C2-1-R, CTQ2015-71955-REDT and MAT2016-77608-C3-1-P) is acknowledged. E. Martínez-Periñán acknowledges funding from Comunidad de Madrid (NANOAVANSENS Program) for financial support.

**References**

1. Gewirth, A. A.; Niece, B. K., Electrochemical Applications of in Situ Scanning Probe Microscopy. *Chem. Rev* **1997,** *97* (4), 1129-1162.

2. Itaya, K., In situ scanning tunneling microscopy in electrolyte solutions. *Prog. Surf. Sci.* **1998,** *58* (3), 121-247.

3. Mirkin, M. V., Peer Reviewed: Recent Advances in Scanning Electrochemical Microscopy. *Anal. Chem.* **1996,** *68* (5), 177A-182A.

4. Toney, M. F., Studies of Electrodes by in Situ X-Ray Scattering. In *Synchrotron Techniques in Interfacial Electrochemistry*, Melendres, C. A.; Tadjeddine, A., Eds. Springer Netherlands: Dordrecht, 1994; pp 109-125.

5. Schumacher, R., Electrochemical interfaces : modern techniques for in-situ interface characterization. Abruña, H. D., Ed. VCH Pub.: New York :, 1991.

6. Osawa, M., Dynamic Processes in Electrochemical Reactions Studied by Surface-Enhanced Infrared Absorption Spectroscopy (SEIRAS). *Bull. Chem. Soc. Jpn.* **1997,** *70* (12), 2861-2880.

7. Ferreira, L. M. C.; Grasseschi, D.; Santos, M. S. F.; Martins, P. R.; Gutz, I. G. R.; Ferreira, A. M. C.; Araki, K.; Toma, H. E.; Angnes, L., Unveiling the Structure of Polytetraruthenated Nickel Porphyrin by Raman Spectroelectrochemistry. *Langmuir* **2015,** *31* (14), 4351-4360.

8. Rodríguez-Calero, G. G.; Conte, S.; Lowe, M. A.; Burkhardt, S. E.; Gao, J.; John, J.; Hernández-Burgos, K.; Abruña, H. D., In situ electrochemical characterization of poly-3,4-ethylenedioxythiophene/tetraalkylphenylene diamine films and their potential use in electrochemical energy storage devices. *J. Electroanal. Chem.* **2016,** *765* (Supplement C), 65-72.

9. Ibañez, D.; Santidrian, A.; Heras, A.; Kalbáč, M.; Colina, A., Study of Adenine and Guanine Oxidation Mechanism by Surface-Enhanced Raman Spectroelectrochemistry. *J. Phys. Chem. C* **2015,** *119* (15), 8191-8198.

10. Fleischmann, M.; Korinek, K.; Pletcher, D., The oxidation of organic compounds at a nickel anode in alkaline solution. *J. Electroanal. Chem. and Inter.Electrochem.* **1971,** *31* (1), 39-49.

11. Martinez-Perinan, E.; Gennari, M.; Revenga-Parra, M.; Abad, J. M.; Mateo-Marti, E.; Pariente, F.; Castillo, O.; Mas-Balleste, R.; Zamora, F.; Lorenzo, E., Highly dense nickel hydroxide nanoparticles catalyst electrodeposited from a novel Ni(II) paddle-wheel complex. *J. Catal.* **2015,** *329*, 22-31.

12. McQuillan, A. J., The discovery of surface-enhanced Raman scattering. *Notes Rec.-The Roy. Soc. J. Hist. Sci.* **2009,** *63* (1), 105.

13. Gao, P.; Gosztola, D.; Leung, L.-W. H.; Weaver, M. J., Surface-enhanced Raman scattering at gold electrodes: dependence on electrochemical pretreatment conditions and comparisons with silver. *J. Electroanal. Chem. and Inter.Electrochem.* **1987,** *233* (1), 211-222.

14. Capilla, A. V.; Aranda ,R. A., Anhydrous Zinc (II) acetate (CH3-COO)2ZN, *Cryst. Struct. Comm.* **1979,** *8*, 3.

15. Clegg, W.; Little, I. R.; Straughan, B. P., Monoclinic anhydrous zinc(II) acetate. *Acta Crystallogr. Sect. C-Struct. Chem.* **1986,** *42* (12), 1701-1703.

16. He, H., A new monoclinic polymorph of anhydrous zinc acetate. *Acta Crystallogr. Sect. E.-Struct Rep.* **2006,** *62* (12), m3291-m3292.

17. Weber, B.; Betz, R.; Bauer, W.; Schlamp, S., Crystal Structure of Iron(II) Acetate. *Z. Anorg. Allg. Chem.* **2011,** *637* (1), 102-107.

18. R. Alcalá, J. F. G., *Rev. Acad. Ciencias* **1973,** *28*, 3.

19. Cotton, F. A.; Rice, C. E.; Rice, G. W., Crystal and molecular structure of anhydrous tetraacetatodichromium. *J. Am. Chem. Soc.* **1977,** *99* (14), 4704-4707.

20. van Niekerk, J. N.; Schoening, F. R. L.; Talbot, J. H., The crystal structure of zinc acetate dihydrate, $Zn(CH_3COO)_2 \cdot 2H_2O$. *Acta Crystallogr.* **1953,** *6* (8-9), 720-723.

21. van Niekerk, J. N.; Schoening, F. R. L., The crystal structures of nickel acetate, $Ni(CH_3COO)_2 \cdot 4H_2O$, and cobalt acetate, $Co(CH_3COO)_2 \cdot 4H_2O$. *Acta Crystallogr.* **1953,** *6* (7), 609-612.

22. Downie, T. C.; Harrison, W.; Raper, E. S.; Hepworth, M. A., A three-dimensional study of the crystal structure of nickel acetate tetrahydrate. *Acta Crystallogr. Sect. B-Struct. Sci.* **1971,** *27* (3), 706-712.

23. De Jesus, J. C.; González, I.; Quevedo, A.; Puerta, T., Thermal decomposition of nickel acetate tetrahydrate: an integrated study by TGA, QMS and XPS techniques. *J. Mol. Catal. A-Chem.* **2005,** *228* (1), 283-291.

24. Siiman, O., Resonance Raman spectra of bis, planar nickel (II) -sulfur ligand complexes. *Inorg. Chem.* **1980,** *19* (10), 2889-2894.

25. Bishop, D. W.; Thomas, P. S.; Ray, A. S., Micro Raman characterization of nickel sulfide inclusions in toughened glass. *Mater. Res. Bull.* **2000,** *35* (7), 1123-1128.

26. Datta, M.; Brown, D. H.; Smith, W. E., The resonance Raman profile of a nickel Schiff base complex at 10 K. *Spectroc. Acta Pt. A-Molec. Biomolec. Spectr.* **1983,** *39* (1), 37-41.

27. Bickley, R. I.; Edwards, H. G. M.; Rose, S. J.; Gustar, R., A raman spectroscopic study of nickel(II) acetate, $Ni(CH_3COO)_2$ and its aqueous and methanolic solutions. *J. Mol. Struct.* **1990,** *238* (Supplement C), 15-26.

## Graphical Abstract